

To Appear in the Astronomical Journal

Deep $3.8\mu\text{m}$ Observations of the Trapezium Cluster¹

Charles J. Lada and August A. Muench

Harvard-Smithsonian Center for Astrophysics

Cambridge, MA 02138

clada@cfa.harvard.edu, gmuench@cfa.harvard.edu

Elizabeth A. Lada

Department of Astronomy, University of Florida

Gainesville, FL 32611

lada@astro.ufl.edu

and

João F. Alves

European Southern Observatory

Karl-Schwartzschild-Strasse 2, 574 Garching Germany

jalves@eso.org

ABSTRACT

We present deep $3.8\mu\text{m } L'$ imaging observations of the Trapezium cluster in Orion obtained with the ESO VLT. We use these observations to: 1) search for infrared excess emission and evidence for protoplanetary disks associated with the faint, substellar population of this young cluster, and 2) investigate the nature and extent of a recently discovered population of deeply embedded sources located in dense molecular gas behind the cluster. We detected 38 L' sources with substellar luminosities. In addition, we detected 24 L' sources that were spectroscopically classified as substellar objects in previous studies. Examining the infrared colors of all these sources we determine an infrared excess fraction of $50 \pm 20\%$ from the $JHK_s L'$ colors for both the luminosity selected and spectroscopically selected substellar samples. This finding confirms the presence of infrared excess, likely due to circumstellar disks, around a significant fraction of the cluster's substellar population, consistent with the indications of earlier observations obtained at shorter (JHK_s) wavelengths. Our deep L' imaging survey also provides new

information concerning the deeply embedded population of young objects located in the molecular cloud behind the cluster and revealed in an earlier L band imaging survey of the region. In particular, our present L' survey doubles the number of sources in the cluster region known to possess extremely red $K-L$ colors. These objects exhibit $K-L'$ colors indicative of deeply buried, possibly protostellar, objects that likely mark the site of the most recent and ongoing star formation in the region. We find the surface density distribution of the deeply embedded population to follow that of the background molecular ridge and to be highly structured, consisting of a string of at least 5 significant subclusters. These subclusters may represent the primordial building blocks out of which the cluster was and perhaps still is being assembled. These observations may thus provide insights into the early stages of cluster formation and appear consistent with recent simulations that suggest that the Trapezium cluster may have formed from numerous but small primordial subclusters.

Subject headings: infrared: stars — stars: low-mass, brown dwarfs, circumstellar matter — open clusters and associations: individual (Trapezium, IC 348)

1. Introduction

The Trapezium cluster is an extremely young and rich embedded cluster at the heart of the Great Orion Nebula. Discovered in early infrared images by Trumpler (1931) and Baade and Minkowski (1937), it is the best studied of all embedded clusters. With age of approximately 10^6 years it remains one of the most important laboratories for investigations of star formation and early stellar evolution in our galaxy. In particular, the cluster has a well determined and well sampled IMF ranging from O stars to substellar objects near the deuterium burning limit (e.g., Muench et al. 2000, 2002; Lucas & Roche 2000; Luhman et al. 2000, Hillenbrand & Carpenter 2000). This enables the statistically significant examination of a number of important astrophysical questions, such as the origin and nature of the IMF, the frequencies of circumstellar disks and protostars in a young population, and the origin of stellar multiplicity in the earliest stages of stellar evolution. Infrared imaging observations of embedded clusters are particularly well suited for addressing such issues (Lada & Lada 2003). In a previous infrared imaging study Lada et al. (2000) obtained extensive $JHKL$ photometry of the cluster. These observations were used both to measure the frequency of infrared excess emission in order to constrain the circumstellar disk fraction in the cluster population and to identify heavily buried protostellar candidates in this young region. They found a relatively high excess fraction of $\sim 80\%$ for the cluster membership, indicating that the vast majority of stars in the cluster were born surrounded by protoplanetary disks. Their observations also revealed a new population of heavily reddened objects deeply buried in molecular gas behind the main cluster. These sources are probably extremely young and mark the location of the most recent and active star formation in the Orion Nebula region. An appreciable fraction of these sources could be protostellar objects.

¹Based on observations collected at the European Southern Observatory, Chile, ESO Program 70.C-0471(A)

For cluster members for which spectra were available, Lada et al. (2000) found that the high excess fraction at L-band ($3.5 \mu\text{m}$) was independent of spectral type and thus stellar mass, for stars later than type A. Indeed, the excess/disk fraction remained high down to the lowest mass objects near the hydrogen burning limit (HBL). This raised the interesting question of whether substellar objects were also born with circumstellar disks. The answer to this question could provide important clues concerning the nature and formation of brown dwarfs (Muench et al. 2001, Reipurth & Clarke 2002). Although the L-band observations of Lada et al. were not sensitive enough to examine a statistically significant sample of objects with substellar luminosities, they did indicate that 8 of 10 objects with spectral types later than M6 exhibited strong L-band excess. Since M6 (e.g., Luhman et al. 1998) is the expected spectral type of a young PMS star at the HBL, this result suggested the possibility that both stellar and substellar objects form surrounded by dusty disks. Indeed, examining deeper *JHK* observations of the Trapezium, Muench et al. (2001) found K_s -band ($2.16 \mu\text{m}$) excesses around a significant fraction ($\sim 65\%$) of the cluster members with substellar luminosities. The fact that many of these brown dwarf candidates with K-band excesses were spatially coincident with optically identified *Hubble Space Telescope* "proplyds" (e.g., Bally, O'Dell & McCaughrean 2000) indicated that these substellar candidates were indeed surrounded by disks. The excess/disk fraction implied by the Muench et al. data was somewhat lower than that derived for the stellar objects in the cluster from the *JHKL* band observations, but higher than predicted by disk models for brown dwarfs which produce smaller amounts of excess emission at K-band (e.g., Walker et al. 2004; Natta et al. 2002)). Moreover, a number of the brown dwarf excess sources were found to lie well below the expected disk locus on the *JHK* color-color diagram, also inconsistent with expectations of circumstellar disk models. Because the magnitude of the infrared excess from a disk increases with wavelength and only very small amounts of dust are required to produce optically thick emission in the $3 - 5 \mu\text{m}$ range, L band is the optimum wavelength for detecting infrared excesses from circumstellar disks using ground-based telescopes (Haisch, Lada & Lada 2001, Wood et al. 2002). To better constrain the excess/disk fraction for the substellar population of the Trapezium cluster requires an extension of the previous L band imaging survey into the brown dwarf regime. Deeper L band observations would also be capable of improving our knowledge and understanding of the deeply embedded population behind the cluster. Do these objects represent a continuation of the cluster forming process that produced the more revealed Trapezium cluster? If so, then their observation may provide interesting insights concerning the nature of the physical mechanism of cluster formation. For example, Scally and Clarke (2002) have argued that the Trapezium cluster could have been formed from the merger of numerous small primordial subclusters. In this case we might expect to directly detect such subclustering in the embedded population. Observation of structure or the lack of it in the embedded population can thus provide important constraints on models of cluster formation. To obtain a sufficiently deep $3 \mu\text{m}$ survey of the Trapezium cluster requires a large telescope, a sensitive array of L band detectors and the best seeing possible. To achieve these goals we obtained observations of a significant portion of the Trapezium cluster with the ESO VLT using an L' ($3.78 \mu\text{m}$) filter under conditions of good seeing. In this paper we present these data, their analysis and implications for understanding the nature of extremely young brown dwarfs and the early stages of cluster formation.

2. Observations and Data Reduction

We obtained deep imaging of the Trapezium cluster in the L' band at $3.78 \mu\text{m}$ using the Infrared Spectrometer And Array Camera, ISAAC (Moorwood et al. 1998), at the VLT UT1 telescope. In order to obtain the best seeing conditions at Paranal the observing program was carried out in Service Mode and data acquisition took place during several nights of good seeing during the southern Summer of 2002. The L' -band sky coverage is shown in Figure 1. Table 1 is a log of the observations and lists the positions, integration times and the measured seeing sizes (FWHM) for each of the fields.

To remove the sky at the L' -band we observed in chopping mode using the VLT chopping secondary mirror in phase with the detector readout. To obtain a difference image the telescope was also nodded 20 arcsec in right ascension in a standard ABBA pattern. The chopping throw was 20 arcsec in right ascension at a frequency of 0.43 s^{-1} . Each on and off image consisted of 9 coadded frames with an integration time of 0.11 seconds per frame. Each nod consisted of 15 chop (on-off) cycles. Each observation consisted of 15 ABBA nod cycles with a random jitter of up to 20 arcsec between ABBA sets. This resulted in a total integration of typically 29.7 minutes for stars observed in both the on and off chop beams. This observing technique gives the best sky subtraction in the L' -band, although it generates a final image that contains many negative sources resulting from sky beam counterparts at the chopping distances. Despite this very few known sources (15) fell into negative images in the reduced chopped image.

Because the chop throw was smaller than an individual image, most stars appeared in both the on and off images and were thus observed twice in each cycle. To take advantage of this each member of the on-off cycle was sky subtracted using the other member of the cycle as a sky to produce two positive images of a target star for each chopped cycle. These images were then flat fielded using sky flats. The flattened images were then appropriately shifted and stacked to produce the final combined image, which typically consisted of a total of 120 observations of each star. This procedure resulted in the production of a final image that was rectangular ($\sim 135 \times 85$ arcsec) in shape. Some of our final combined images contained only 118 observations since occasional problems with the chopping secondary resulted in the production elongated images on some frames and the few observations with such poor images were discarded before the final image was constructed. Figure 2 displays the combined chopped L' band image for one of our fields (L5) and illustrates the quality of the final images. The seeing was typically below 0.5 arcsec.

Sources were identified by visual inspection of the VLT chopped images and by comparison to the locations of sources known from published near-infrared catalogs (e.g., Muench et al 2002, Hillenbrand & Carpenter 2000). Our final catalog consisted of 424 sources with measurable L' photometry; indeed, only 15 known sources were not detected due to negative chop images while 7 bright sources were saturated. By comparison to ground-based JHK surveys we find that we detected $\sim 98\%$ of the known sources brighter than $H = 16$ (see also Figure 3b). Further, 15 new L' -only sources were identified with the vast majority of them projected along the OMC-1 cloud core. Last, ~ 100 individual sources appeared on two or more VLT images (see Figure 1), yielding quality checks on the photometric and positional accuracy of our final catalog.

The IRAF APPHOT package was used to obtain aperture photometry at a large range of radii (2–12

pixels) and with a sky annulus from 12–22 pixels. Corresponding aperture corrections were calculated using the MKAPFILE routine and 10-20 bright sources for each VLT image, although the images’ relatively similar PSFs yielded similar corrections. For this reason, we chose the 8 pixel aperture photometry for all sources, corresponding to a beamsize of $1.136''$ and a typical aperture correction of ~ -0.13 magnitudes. The 8 pixel photometry of 13 sources were affected by negative chop images and/or bright stars in the wings of their PSFs; their photometry was adjusted to an appropriately smaller beamsize. Zeropoint calibration was performed using standard star observations obtained on 3 of the 4 queue observing nights, and photometric zeropoint offsets between frames as revealed by sources in overlap images were removed by cross-calibration to the photometry of the L1 position. Our quoted photometric accuracy as derived from overlap sources is $\sim 5\%$.

Sources were placed onto the 2MASS astrometric grid using plate solutions derived with IRAF routine CCMAP from 30-60 sources on each reduced image. Formal rms errors of these solutions were $\sim 0.1''$; however, sources in overlap regions reveal a smaller relative scatter of order $0.05''$. The final catalog is available in electronic format with Table 2 representative of its contents. To preserve positional information lost in the astrometric plate solutions, we provide both equatorial coordinates and pixel positions of each source (on a specific VLT image). Sources are also cross-referenced to the FLWO-NTT (Muench et al 2002), Hillenbrand & Carpenter (2000) and Hillenbrand (1997) identifications.

3. Results and Discussion

3.1. Color-Magnitude Diagrams: Defining the Substellar Sample

In order to describe the population of L' sources in our survey region, illustrate the sensitivity of our VLT observations, and select the candidate substellar population in the cluster we present the $K-L'$ vs K and $H-K$ vs H color-magnitude diagrams (CMDs) in Figure 3. A total of 400 sources are detected and resolved in K and L' passbands; these are plotted in Figure 3a. Most sources have $K-L' < 2.0$; however, a significant population of sources have much larger colors, with a handful of sources characterized by extremely red colors (i.e., $5 \leq K-L' \leq 6$ magnitudes) suggesting reddenings up to $A_V \sim 100$. It is unclear if the inferred reddenings to these extreme sources are due to pure dust extinction or strong infrared excess emission of the kind that is often associated with protostellar objects, since the reddest of these are not detected at J or H bands.

Similar to Lada et al. (2000), we define the depth of our survey by our ability to detect the photospheres of cluster members. In Figure 3b we plot the $H-K$ vs H color-magnitude diagram for all sources known from previous deep IR surveys within the boundaries of the VLT L' survey. Presuming that the H magnitude of these sources is primarily photospheric, we clearly detect the vast majority of sources down to $H \sim 16$, below which our observations are quite incomplete. Alternately, we are sensitive to the photosphere of a 1 Myr brown dwarf ($0.075M_{\odot}$; $H_0 = 13.54$; Baraffe et al 1998) seen through 20 visual magnitudes of extinction.

Muench et al. (2001) defined a sample of Trapezium sources that were postulated to be sub-stellar based on their unreddened H band luminosity from the 1 Myr isochrone of Baraffe et al. (1998). The validity of that CMD analysis was bolstered by the fact that the luminosity selected sources were on the whole fainter than members with spectral types earlier than M6. Following Muench et al. (2001), we use the H vs $H-K$ color-magnitude diagram to identify candidate brown dwarfs in the Trapezium cluster by comparing their infrared luminosities to the predictions of the Baraffe et al. models. We consider all sources whose dereddened luminosities are less than the predicted luminosity of the HBL for the adopted age (10^6 yrs) and distance (400 pc) of the cluster. By considering all sources below the extrapolated reddening vector for the HBL we identify 38 sources as substellar candidates in our VLT fields. However we note that this sample represents an upper limit to the true number of substellar cluster members that we detected at L' since we have not accounted for background/foreground field star contamination which is predicted to be significant at these faint magnitudes. For example, Muench et al. (2002) estimated, by combining observations of control fields near but off the cluster and a model of the extinction distribution produced by the molecular cloud, that field stars account for as much as 20-30 % of the objects in this magnitude range.

3.2. Color-Color Diagrams: Measuring the Infrared Excess Fraction

In earlier studies Lada et al (2000) and Muench et al (2001) used JHK_L and JHK_s color-color (CC) diagrams, respectively, to diagnosis the presence of infrared excess due to disks around stellar and candidate substellar members of the Trapezium Cluster. We now extend their analysis to include high dynamic range VLT L' data to better assess the infrared excess fraction across the HBL and into the substellar regime. In Figure 4 we present the JHK_s and $JHK_s L'$ infrared CC diagrams for the VLT L' Trapezium sources. There are a total of 345 sources with $JHKL'$ photometry. Sources represented by filled circles are the 38 luminosity selected substellar candidates from the H vs $H-K$ color-magnitude diagram. Plotted for comparison is the intrinsic locus for dwarfs taken from a merger of optical and IR colors from Winkler (1997), Kenyon & Hartmann (1995), Bessell & Brett (1988) and Leggett (1992). Reddening vectors (Whittet 1989) for the giant branch and M6 and M9 dwarfs are also shown.

Although many sources display colors consistent with reddened photospheric colors, a large fraction (50% and 67%, respectively) display infrared excess relative to the M6 reddening vector on both the JHK and $JHKL'$ CC diagrams. As expected, the excess fraction is found to be higher in the latter CC diagram. For the candidate 10^6 year old substellar population we expect most objects to have spectral types of M6 or later (Luhman et al. 1998). Since most of the stars plotted in Figure 4 are more luminous than the HBL, and thus likely to be earlier than M6, those that appear in the infrared excess region of the CC diagrams (Lada & Adams 1992) must be characterized by significant $H-K$ and $K-L'$ excesses. Identifying infrared excess for substellar objects, particularly in the $JHKL'$ CC diagram, is a much more difficult task than for it is for stars above the HBL. This is because the range of intrinsic $K-L'$ colors for M6-M9 dwarfs is relatively large and, in fact, comparable to the entire range in intrinsic $K-L'$ colors for all earlier spectral types and moreover larger than the corresponding $H-K$ intrinsic color spectrum. Nevertheless, a significant fraction (42%) of the substellar candidates fall to the right of the M9 reddening vector on the $JHKL'$ CC diagram and

consequently have significant $K-L'$ excess. A similarly high fraction (44%) of substellar candidates display excesses in the JHK CC diagram with respect to the M9 reddening vector. This relatively high fraction from the JHK CC diagram is roughly consistent with the findings of Muench et al. (2001) but inconsistent with expectations of disk models, as mentioned earlier.

We also note that about 1/3 of the luminosity selected substellar objects have colors apparently consistent with reddened stars of spectral type earlier than M6. Some of these sources are likely field stars. For others their relatively blue colors could be the result of photometric uncertainties in the observed colors. Moreover, the JHK observations were obtained at a different epoch than the L' observations, and consequently variability, if present, could contaminate some of the $K-L'$ colors. In addition, this result is also reminiscent of the recent spectroscopic study of Slesnick, Hillenbrand and Carpenter (2004) who found a similar sized fraction of luminosity selected substellar candidates in the Trapezium cluster to be characterized by spectral types earlier than the nominal M6 substellar boundary. The nature of this apparently subluminescent stellar population is unknown. Both our CC diagrams also show sources which fall into relatively 'forbidden' regions of the diagrams. In Figure 4a there is a population of sources with very red $H-K$ colors and relatively blue $J-H$ colors. Some of these same sources also appear to be unexpectedly blue in $K-L'$ color in Figure 4b; as was discussed in Lada et al (2000) and Muench et al (2001) many of these sources are 'proplyds' (O'dell Wen & Hu 1993) and their colors are possibly contaminated by scattered light and/or emission from the photoionized envelopes surrounding the underlying disks.

To further investigate the behavior of the infrared excess/disk fraction across the HBL we divided the source distribution in the $H-K$ vs H CMD into 7 luminosity bands, approximating equal sized steps in unreddened H magnitude and logarithmic mass using predicted H_0 magnitudes from the the Baraffe et al (1998) 1 Myr isochrone. The magnitude bins and corresponding predicted masses are listed in Table 3. We further constructed an extinction limited sample by including in each bin only sources with extinctions $A_V \leq 20$. The fraction of sources in each luminosity selected bin displaying infrared excess greater than their formal 1 sigma photometric errors was counted in the corresponding JHK , $JHKL'$ and HKL' color-color diagrams. The M6 spectral type boundary was used to calculate the infrared excess fraction for all bins. In addition for bins 5-7 the infrared excess fraction was also calculated using the M9 boundary, since these bins are likely to contain brown dwarfs. The corresponding excess fractions are listed in Table 3, while in Figure 5 we plot these fractions as a function of the luminosity bin center.

Clearly, Trapezium sources display excess at all magnitudes and in all diagrams with the $JHKL'$ and HKL' diagrams giving nearly identical results. As already shown by Lada et al (2000), the fraction of bright sources displaying excess is larger when using $K-L$ as a color diagnostic ². Yet as H_0 increases into the fiducial brown dwarf regime (Band 5-7), the excess fraction traced by $K-L'$ appears to decrease, although the uncertainty in the excess fraction increases due the larger range of intrinsic $K-L$ colors for M6-M9

²The fraction of bright ($H < 12$) sources showing excess in these diagrams appears lower than published in Lada et al (2000) for two reasons. First, the L' ($3.8\mu\text{m}$) bandpass of the VLT data yields redder photospheric colors than the L ($3.5\mu\text{m}$) bandpass of the FLWO data making the identification of a infrared excess somewhat more difficult at L' for late spectral types. Second, we are consistently counting from the M6 rather than the M5 boundary used Lada et al (2000)

sources. Note, our results for band 7 are likely upper limits because of incompleteness, which manifests itself in our ability to detect only those faint sources with disks. This decrease in $K-L$ excess fraction is *opposite* the behavior traced by $H-K$, which increases for the brown dwarf luminosity bins and recovers the $> 50\%$ excess fraction quoted by Muench et al (2001). The physical origin of this difference in behavior is unknown. Nonetheless, the L' measurements indicate a relatively high infrared excess and likely disk fraction for the substellar population of this cluster. Merging the results for luminosity bands 6 and 7 from Table 2 we estimate an infrared excess fraction for the substellar population of the cluster of $50 \pm 20\%$ from the $JHKL'$ diagram. Our measurements also hint that the disk fraction for the substellar population is somewhat lower than that of the stellar population. However, considering the uncertainties and the possible effects of field star contamination, one cannot yet draw a firm conclusion about the presence of a decrease in excess fraction for the substellar population in the cluster.

There are a number of limitations to our estimate of the excess/disk fraction for the substellar population from our VLT L' data. First, our measurements of the excess fraction are incomplete for the lowest luminosity bin resulting in an overestimate for the excess fraction in that bin. Second, the lack of specific knowledge about the intrinsic infrared colors of the objects results in the relatively large quoted uncertainties ($\pm 20-30\%$) for our estimate of the excess fraction of the luminosity selected substellar candidates. The lack of knowledge of source intrinsic color also presumably affects the derived excess fraction at brighter magnitudes as well since an M0 star, for example, will require 0.3 magnitudes of $K-L$ excess in order to be counted as an excess source using the M6 boundary. Given that any age spread for Trapezium members will result in a mix of mass (as traced by spectral type) as a function of luminosity, assigning a single spectral type boundary only acts to underestimate the true excess fraction. In addition we have not attempted to correct for foreground/background source contamination which is likely present for these faint sources. The presence of such contaminating sources also results in an underestimate of the true excess fraction.

3.3. Infrared Excess Fraction for a Spectroscopically Selected Substellar Sample

Liu et al. (2003) have shown that a more complete assessment of infrared excess in substellar sources can be made if the spectral types and thus the intrinsic colors of the stars are individually known and taken into account in measuring infrared excess emission. Combining spectra with infrared $JHKL'$ photometry of substellar candidates in Taurus and IC 348, Liu et al. (2003) derived a $K-L'$ band excess/disk fraction of 77% for stars they selected with late spectral types. This was a significantly higher fraction than that ($\sim 33\%$) inferred from analysis of the $JHKL'$ CC diagram for the same sources. Therefore it would be extremely valuable to examine the infrared colors of those substellar candidates in the Trapezium that have been spectroscopically classified so that their intrinsic infrared colors are known.

Over the past few years various workers have collected spectra of faint stars in the Trapezium cluster (i.e., Hillenbrand, 1997; Lucas et al. 2001; Luhman et al. 2000; Slesnick, Hillenbrand and Carpenter, 2004). From these studies we find a total of 24 objects with spectral types of M6 or later that were also detected in our L' images. In Figure 6 we show the JHK_s and JHK_sL' CC diagrams for this spectroscopically

selected sample of substellar candidates. With the assumption of dwarf colors for the spectroscopically selected sample we can convert the spectral types to intrinsic substellar colors. With knowledge of the spectroscopically derived intrinsic $H - K_s$ colors of the stars, we derive an excess fraction of $70\% \pm 15\%$ from comparison with their observed $H - K_s$ colors. This is in excellent agreement with the fraction derived by Muench et al. (2001) from photometry using the JHK_s CC diagram and roughly consistent with our estimate based solely on JHK_s photometry of sources detected at L' . However this value is higher than would be expected by traditional disk models. Using the $K_s - L'$ data we derive in a similar manner an excess fraction of $52\% \pm 20\%$ for the spectroscopically selected substellar candidates. Although this represents a significant excess fraction, the calculated value is formally lower than both the fraction derived by Liu et al. (2003) for Taurus and IC 348 using $K - L'$ colors and the fraction derived for the same sources from our JHK_s colors. However given the relatively large uncertainties it is difficult to assess the significance of this difference. Moreover it is difficult to compare the results between our spectroscopically selected Trapezium sample and the Liu et al. L' IC 348 plus Taurus sample, since neither can be considered complete and may not even be fully representative of the entire substellar populations in the respective clouds. Finally, an additional uncertainty may arise from our assumption of dwarf colors for these objects since they are expected to have lower surface gravities than field dwarfs. Theoretical models predict that lower surface gravity stars should have somewhat bluer $K - L$ colors, leading to an underestimate of the excess fraction when assuming dwarf colors (Liu et al. 2003). We find that these same model atmospheres (i.e., Baraffe et al. 2002) predict slightly bluer $J - H$ colors and no change in the $H - K$ colors for lower surface gravity atmospheres with the result that the excess fraction derived assuming dwarf colors is not significantly altered. The relatively large excess fraction derived from JHK colors is unexpected and as speculated earlier by Muench et al. (2001) may be the result of scattered light or emission from the photoionized envelopes of the disks, since many of the sources with these colors appear to be proplyds.

4. Deeply Embedded Objects and Protocluster Structure

The L band imaging survey of Lada et al (2000) resulted in the identification of a previously unrecognized population of heavily reddened objects toward the Trapezium cluster. Seventy-eight sources were found to have large $K - L$ colors (i.e., $K - L > 1.5$ mag.) suggestive of objects deeply embedded in molecular gas and dust. For example, for a normal interstellar reddening law (e.g, Mathis 1990) this would correspond to $A_V > 27$ magnitudes for a typical naked field star seen through the cloud and approximately $A_V > 15$ magnitudes for a young star with a circumstellar disk. The spatial distribution of these red objects was found to differ from that of the bulk of the (less reddened, $A_V \sim 5$ mag.) cluster membership, but to be similar to that of the dense molecular ridge located behind the cluster. The molecular ridge has long been known to be a site of star formation, harboring the massive protostellar objects IRC2 and BN-KL. The L band survey indicated that the star formation activity in the ridge was considerably more active than previously suspected. Many of the new and heavily buried sources were found to be characterized by the extreme infrared excess in the $JHKL$ CC diagram often observed in protostars.

Our deeper L' observations have revealed 73 objects with $K - L' > 1.5$ magnitudes and 40 with $K -$

$L' > 2.0$ magnitudes within the six fields we imaged. Within these fields 25 objects were identified as having $K-L > 1.5$ magnitudes in the earlier survey by Lada et al. (2000) and 48 are newly identified members of the deeply embedded population (most of which were below the L band sensitivity limit in the previous survey). Together with the earlier data of Lada et al., our observations indicate that that deeply embedded population consists of approximately 126 members, roughly 20% the size of the foreground and more revealed Trapezium cluster.

The VLT sources with $K-L' > 1.5$ magnitudes are plotted as filled squares in Figure 1. These sources form a tight distribution that more or less follows the molecular ridge (see figure 7 of Lada et al. 2000 and also Johnstone & Bally 1999). The extremely high extinctions inferred for these sources coupled with their relatively high surface density, clearly indicates that the vast majority are embedded in the cloud and not reddened background field stars. Moreover, the reddest of these sources have $K-L'$ colors suggestive of visual extinctions of up to 100 magnitudes! Such extreme extinctions typically arise from dense envelopes of deeply embedded protostellar objects and not from the more distributed dense gas of a molecular cloud core. As suggested by Lada et al (2000) many such objects are likely protostellar in nature and still in the process of forming. In addition our new observations revealed 15 previously undetected L' only sources, plotted as filled diamonds in Figure 1. As seen in this figure twelve of these are found coincident with the molecular ridge and are likely additional members of the deeply embedded population. The brightest of these is the source vlt-129 ($L' = 10.98$) which lies $28''$ southwest of the BNKL and is characterized by a $K-L'$ color of > 6 magnitudes.

The population of deeply embedded objects (DEOs) traces the most recent epoch of star formation in the Trapezium cluster region. The spatial structure of the deeply embedded population possesses an imprint of the physical processes responsible for its creation and thus can provide important insights into the earliest phases of cluster formation process. In their study of embedded clusters Lada & Lada (2003) found that embedded clusters could be characterized by two basic structural types. Type 1 clusters exhibited hierarchical spatial structure characterized by significant sub-clustering in their surface density distributions. Such highly structured systems are thought to be a signature of the important role of turbulence in the evolution of molecular gas to form stars. Type 2 clusters exhibited centrally-concentrated structure typically characterized by relatively smoothly varying radial surface density profiles. Such centrally condensed structures are thought to be a signature of the global dominance of gravity in the formation of the stellar system. It is not clear whether these two types of structures represent two different primordial structures or two differing evolutionary states of an embedded cluster. Most embedded clusters appear to be type 2 structures, yet most progenitor molecular clouds appear to be filamentary in shape and highly structured, at least on large scales. This perhaps suggests that centrally condensed type 2 structures may form from more structured type 1-like initial configurations. Indeed, in a recent numerical simulation of cluster formation from a turbulent cloud, Bate, Bonnell and Bromm (2003) found that filamentary clouds could form stars which fall together to form small groups within a larger cluster forming system. Earlier numerical simulations by Scally and Clarke (2000) have suggested that relaxed, centrally condensed stellar clusters can form from the merger of smaller subclusters. They suggested that the Orion Nebula Cluster (and by implication the Trapezium cluster which forms its inner core) could have formed from the merger of subclusters provided that these subclusters were

relatively small and numerous.

Existing surface density maps of the Trapezium cluster suggest that it is a type 2 or centrally concentrated embedded cluster (Hillenbrand & Hartmann 1998; Lada et al. 2000; Scally & Clarke 2002). In Figure 7 we plot the surface density distribution of the embedded population (contours) along with that of the less extinguished members of the Trapezium cluster (grey scale). Our deeper observations allow us to map these distributions at higher angular resolution than previously possible. The deeply embedded population is found to be significantly structured appearing to consist of five subclusters oriented more or less along the filamentary molecular ridge. The basic parameters of the subclusters are listed in Table 4. These five subclusters account for approximately 55% of the stars in the deeply embedded population. If the formation of the deeply embedded population is a continuation of the same physical process that produced the foreground Trapezium cluster, then it is tempting to identify the subclusters with the fundamental units or building blocks out of which the cluster continues to be assembled. If this interpretation is correct, then it suggests that a centrally condensed cluster may be formed from the merger of smaller subclusters which themselves formed initially in filamentary dense molecular gas in accord with the suggestion of Scally and Clarke (2002).

The deep infrared observations also allow us to examine the structure of the foreground Trapezium cluster in more detail than previously possible. Infrared *JHK* CC diagrams (see Figure 4 and Lada et al. 2000, Figure 8) show that the bulk of the Trapezium cluster is characterized by extinctions less than about 5-6 magnitudes. Therefore to map the structure of the foreground Trapezium cluster we plotted in Figure 7 the spatial surface density distribution of stars with $J-H < 1.5$ magnitudes (corresponding to A_V s of approximately 10 magnitudes or less). The surface density map of the cluster is dominated by a strong central peak at the site of the Trapezium ($N_* = 6000 \text{ pc}^{-2}$), in agreement with previous studies. However, our higher resolution map reveals additional significant structure in the cluster. Three secondary peaks with peak surface densities of 3000 pc^{-2} or greater are found to the north and east of the primary peak. Together the four subclusters account for about 28% of the total population of the foreground cluster. The basic parameters of these subclusters are also listed in Table 4. These secondary peaks are reminiscent of the satellite subclusters observed in IC 348 (Lada & Lada 1995) another otherwise highly centrally concentrated embedded cluster.

Comparison of the embedded source and cluster surface density distributions generally confirms earlier results in that, for the most part, the two populations have different spatial distributions which are offset from one another. However, one peak in the DEO distribution is coincident with the primary peak in the Trapezium cluster distribution. Although significant this peak in the DEO distribution may not be in fact as prominent as it appears in the map since at least 3 of the sources in it are foreground proplyds with very red colors. In addition the strongest peak in the DEO distribution, which is coincident with BN-KL region, is near, but offset from the second strongest peak in the foreground cluster distribution. Thus it appears that at least some of the structure in the foreground Trapezium cluster reflects the more primordial structure in the background embedded population. These observations suggest that the foreground Trapezium cluster is still sufficiently young that it is not yet fully relaxed into a centrally condensed, isothermal-like stellar distribution. Moreover, the presence of structure in the embedded source population suggests that the cluster

will need to undergo still more structural evolution in order to eventually incorporate the presently embedded sub-clusters and form a fully relaxed and centrally concentrated stellar system.

5. Summary and Conclusions

We have obtained deep $3.8 \mu\text{m } L'$ observations of the Trapezium cluster using the ESO VLT. We have imaged a significant fraction of the inner $5' \times 5'$ region of the cluster. Our observations extend the previous L band survey of Lada et al. (2000) to fainter cluster members and include approximately 38 objects with luminosities below that expected for cluster members at the HBL. In addition, we detected 24 objects with previously known spectral types that are later than that corresponding to the HBL (M6). Combining our deep L' data with previous JHK_S observations we have examined the frequency of infrared excess emission among the candidate substellar population. We derive an infrared fraction of $50 \pm 20\%$ for the substellar population from analysis of the $JHK_S L'$ colors of both luminosity selected and spectroscopically selected samples of substellar candidates. This result suggests a significant disk fraction for substellar sources, consistent with earlier results for this and other clusters (Muench et al. 2001; Liu et al. 2003). The presence of disks around substellar objects provides evidence that the formation mechanism for brown dwarfs and more massive stars is a physically similar process as has been previously argued (Muench et al. 2001, Liu et al. 2003). Due to issues of completeness and contamination of the sample by foreground/background stars we cannot determine the true excess/disk fraction for the substellar population and it is therefore not clear whether our measured value of $\sim 50\%$ for substellar objects is significantly different from the $\sim 65\%$ fraction found for a complete and representative sample of the stellar members of the cluster from $JHK_S L'$ observations.

Our observations also confirm that a number of substellar candidate sources possess unusual colors on the JHK_S CC diagram. This is true for both luminosity selected and spectroscopically selected substellar candidates. These sources exhibit significantly larger infrared $H-K_S$ excesses than predicted by conventional disk models and thus appear redder for their $J-H$ color. Moreover, a few of these sources exhibit K_S-L' colors that are two blue for their $J-H$ color and do not appear as K_S-L' excess sources on the $JHK_S L'$ CC diagram. The origin of these anomalous colors is unclear. Photometric errors, source variability and perhaps contamination by protoplanetary emission may all contribute to explain these unusual characteristics.

Our deep L' observations also reveal a significant number of new members of the deeply embedded population of young objects which lies buried in the molecular cloud behind the cluster. As a whole this embedded population represents the location of the most recent star forming events in the Trapezium region. We find the surface density distribution of the deeply embedded population to follow that of the background molecular ridge and to be highly structured, consisting of a string of at least 5 significant sub-clusters. If the embedded population represents a continuation of the star formation process responsible for the creation of the more revealed Trapezium cluster, then these embedded sub-clusters are likely representative of the primordial building blocks out of which the cluster was and perhaps is still being assembled. Additional evidence for this possibility is found in high resolution map of the surface density distribution of the Trapezium

cluster itself which shows, in addition to a strong and centrally concentrated peak, significant substructure in the form of small satellite subclusters similar to those in the background cloud. These findings are generally consistent with the suggestion of Scally and Clarke (2002) that the Trapezium cluster could have been assembled from the merger a large number of small (< 50 stellar members) subclusters over the past 10^6 years.

We are grateful to Richard J. Elston for useful advice and suggestions pertaining to the image reduction and analysis and to Kevin Luhman for useful discussions. EAL acknowledges support from NSF grants, AST97-3367 and AST02-02976 to the University of Florida.

REFERENCES

- Baade, W. & Minkowski, R. 1937, *ApJ*, 86, 119
- Bally, J., O'Dell, C. R., & McCaughrean, M. J. 2000, *AJ*, 119, 2919
- Baraffe, I., Chabrier, G., Allard, F., & Hauschildt, P. H. 1998, *A&A*, 337, 403
- Baraffe, I., Chabrier, G., Allard, F., & Hauschildt, P. H. 2002, *A&A*, 382, 563
- Bate, M. R., Bonnell, I. A., & Bromm, V. 2003, *MNRAS*, 339, 577
- Bessell, M. S. & Brett, J. M. 1988, *PASP*, 100, 1134
- Haisch, K. E., Lada, E. A., & Lada, C. J. 2001a, *AJ*, 121, 2065
- Hillenbrand, L. A. 1997, *AJ*, 113, 1733
- Hillenbrand, L. A. & Hartmann, L. W. 1998, *ApJ*, 492, 540
- Hillenbrand, L. A. & Carpenter, J. M. 2000, *ApJ*, 540, 236
- Johnstone, D. & Bally, J. 1999, *ApJ*, 510, L49
- Kenyon, S. J. & Hartmann, L. 1995, *ApJS*, 101, 117
- Lada, C. J. & Adams, F. C. 1992, *ApJ*, 393, 278
- Lada, C. J., Muench, A. A., Haisch, K. E., Lada, E. A., Alves, J. F., Tollestrup, E. V., & Willner, S. P. 2000, *AJ*, 120, 3162
- Lada, C. J. & Lada, E. A. 2003, *ARA&A*, 41, 57
- Lada, E. A. & Lada, C. J. 1995, *AJ*, 109, 1682.
- Leggett, S. K. 1992, *ApJS*, 82, 351
- Liu, M. C., Najita, J., & Tokunaga, A. T. 2003, *ApJ*, 585, 372
- Lucas, P. W. & Roche, P. F. 2000, *MNRAS*, 314, 858
- Lucas, P. W., Roche, P. F., Allard, F., & Hauschildt, P. H. 2001, *MNRAS*, 326, 695
- Luhman, K. L., Briceno, C., Rieke, G. H., & Hartmann, L. 1998, *ApJ*, 493, 909
- Luhman, K. L. 1999, *ApJ*, 525, 466
- Luhman, K. L., Rieke, G. H., Young, E. T., Cotera, A. S., Chen, H., Rieke, M. J., Schneider, G., & Thompson, R. I. 2000, *ApJ*, 540, 1016

- Mathis, J. 1990, *ARA&A*, 28, 37.
- Moorwood, A., et al. 1998, *The Messenger*, 94, 7
- Muench, A. A., Lada, E. A., & Lada, C. J. 2000, *ApJ*, 533, 358
- Muench, A. A., Alves, J., Lada, C. J., & Lada, E. A. 2001, *ApJ*, 558, L51
- Muench, A. A., Lada, E. A., Lada, C. J., & Alves, J. 2002, *ApJ*, 573, 366
- Natta, A., Testi, L., Comerón, F., Oliva, E., D’Antona, F., Baffa, C., Comoretto, G., & Gennari, S. 2002, *A&A*, 393, 597
- O’Dell, C. R., Wen, Z., & Hu, X. 1993, *ApJ*, 410, 696
- Reipurth, B. & Clarke, C. 2001, *AJ*, 122, 432
- Scally, A. & Clarke, C. 2000, *MNRAS*, 334, 156.
- Slesnick, C. L., Hillenbrand, L. A., & Carpenter, J. M. 2004, *ApJ*, in press (astro-ph/0404292)
- Trumpler, R. J. 1931, *PASP*, 43, 255
- Walker, C., Wood, K., Lada, C. J., Robitaille, T., Bjorkman, J. E., & Whitney, B. 2004, *MNRAS*, in press (astro-ph/0403276)
- Whittet, D. C. B. 1988, *Dust in the Universe*, 25
- Winkler, H. 1997, *MNRAS*, 287, 481
- Wood, K., Lada, C. J., Bjorkman, J. E., Kenyon, S. J., Whitney, B., & Wolff, M. J. 2002, *ApJ*, 567, 1183

Fig. 1.— Spatial distribution of VLT detected sources in the Trapezium. The area covered by individual chopped pointings are outlined and labeled L1...L6. Known sources (from the Muench et al 2002 catalog) are plotted as open symbols, while those detected and photometered in the VLT L' data are shown as filled circles. Open circles containing crosses were either saturated or affected by negative images in the chopped data. Large grey filled diamonds mark the locations of 15 new sources detected only in the VLT L' band data.

Fig. 2.— VLT L' band image of the L5 pointing in greyscale using a logarithmic stretch. Sources detected only at $3.8\mu\text{m}$ are surrounded by white squares. Note the excellent image quality and high spatial resolution, which allows excellent photometry even in the crowded region near the central OB stars (image left).

Fig. 3.— Infrared color-magnitude diagrams for sources in the VLT Trapezium L' images. A) $K-L'$ vs K ; B) $H-K$ vs H . The location of all sources detected in K and L' bands are plotted in (A). Sources currently undetected at H band are plotted as open circles; Saturated sources were excluded. The locations for all known sources detected in the J, H and K bands in the fields observed by the VLT are plotted in (B), excluding sources that fell into chopped negative regions. Sources detected at L' are shown as filled circles. The source distribution in this CMD was divided into 7 bands based on the sources' unreddened H band magnitudes; each luminosity band approximates equal sized steps in logarithmic mass using the 1 Myr isochrone from Baraffe et al. (1998) and a distance of 400 pc. See text. In addition reddening vectors with lengths of $A_V = 35$ and 20 magnitudes are plotted in A and B, respectively.

Fig. 4.— Infrared color-color diagrams for sources in the VLT Trapezium L' images. A) $J-H$ vs $H-K$; B) $J-H$ vs $K-L'$. Substellar candidate sources selected from the CM diagram are indicated by open circles. Colors are compared to the dwarf star locus (see text references).

Fig. 5.— Fraction of sources displaying excess in color-color diagrams as a function of un-reddened H band magnitude. Excess fractions were calculated for the luminosity bands defined in Figure 3b. Results for two color-color diagrams ($JHKL'$ and JHK) and two intrinsic color boundaries (M6 & M9) are shown. The last bin likely represents an upper limit due to incomplete detections at L' .

Fig. 6.— Infrared color-color diagrams for spectroscopically selected substellar candidate sources detected at L' . Different symbols correspond to the different spectral types.

Fig. 7.— Maps of the surface density distribution of the deeply embedded object population (red contours) and the more foreground and less extincted Trapezium cluster (grey scale). For the cluster only members with $J-H$ colors < 1.5 magnitudes (roughly corresponding to $A_V \leq 8-10$ magnitudes) are plotted. For the deeply embedded population all sources with $K-L$ colors > 1.5 magnitudes (roughly corresponding to $A_V > 15-26$ magnitudes) are plotted. Contours that trace the deeply embedded population start at a surface density of $1000 \text{ stars pc}^{-2}$ and increase in steps of $500 \text{ stars pc}^{-2}$. The grey scale contours that trace the cluster start at $500 \text{ stars pc}^{-2}$ and increase in steps of $500 \text{ stars pc}^{-2}$.

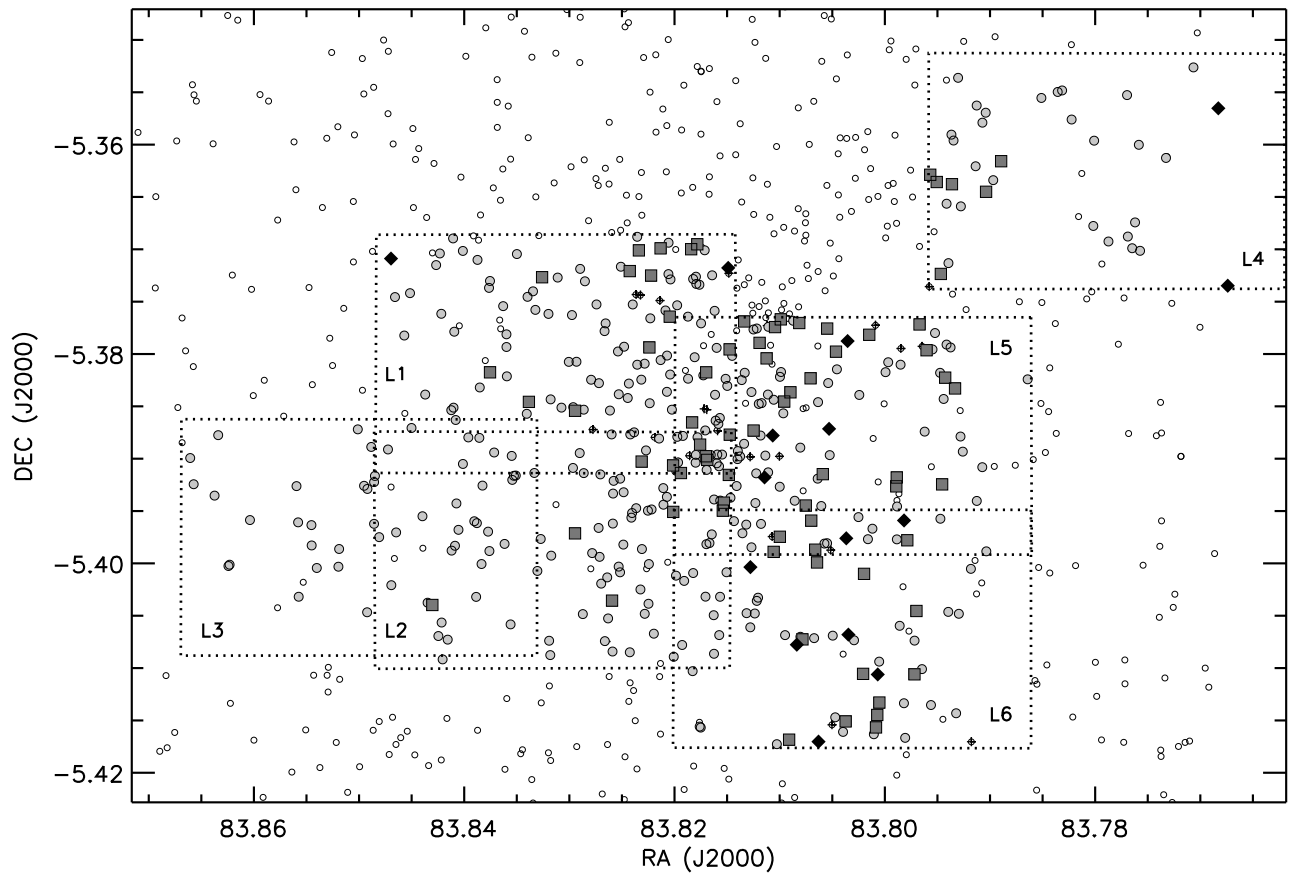
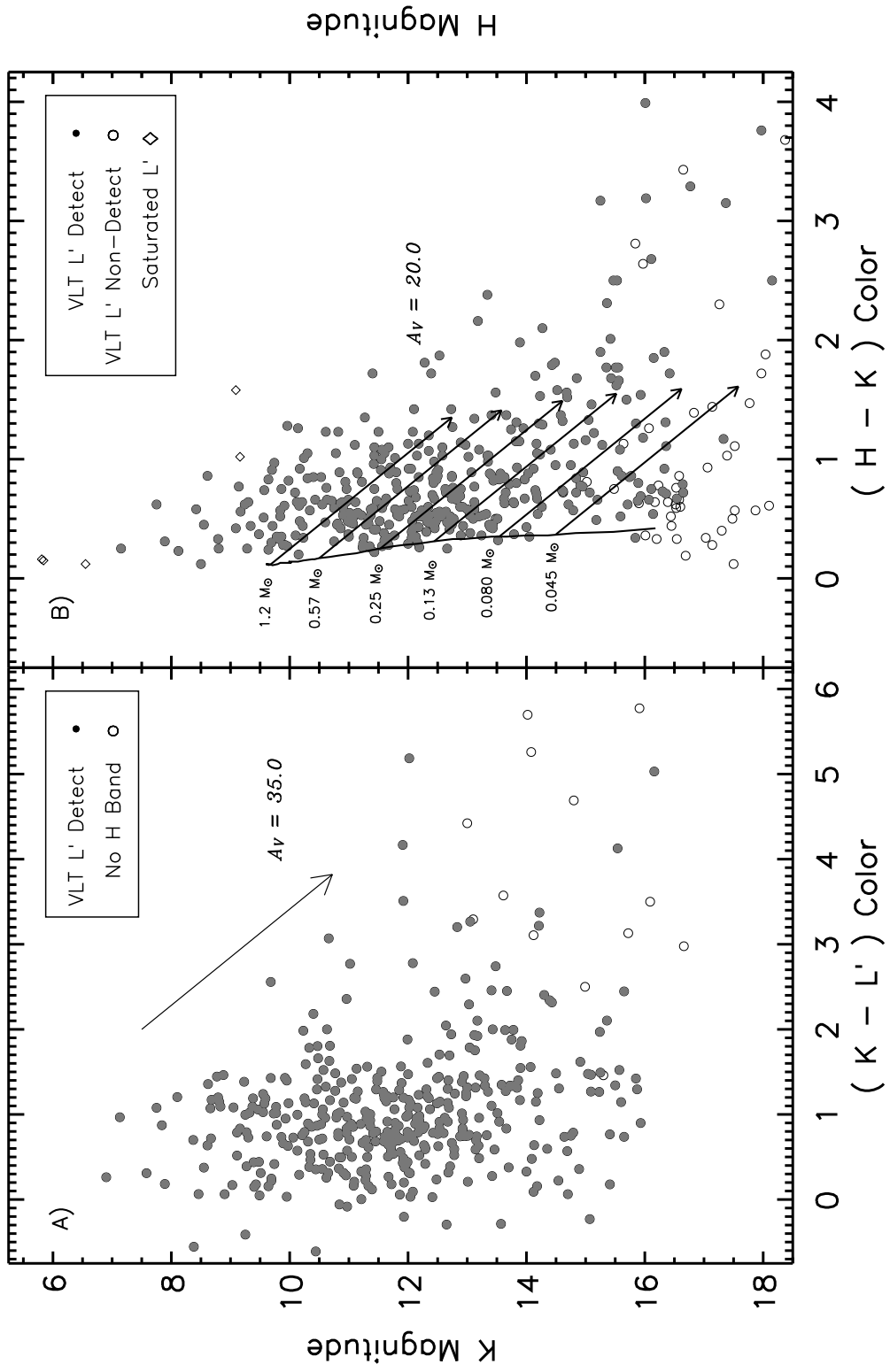
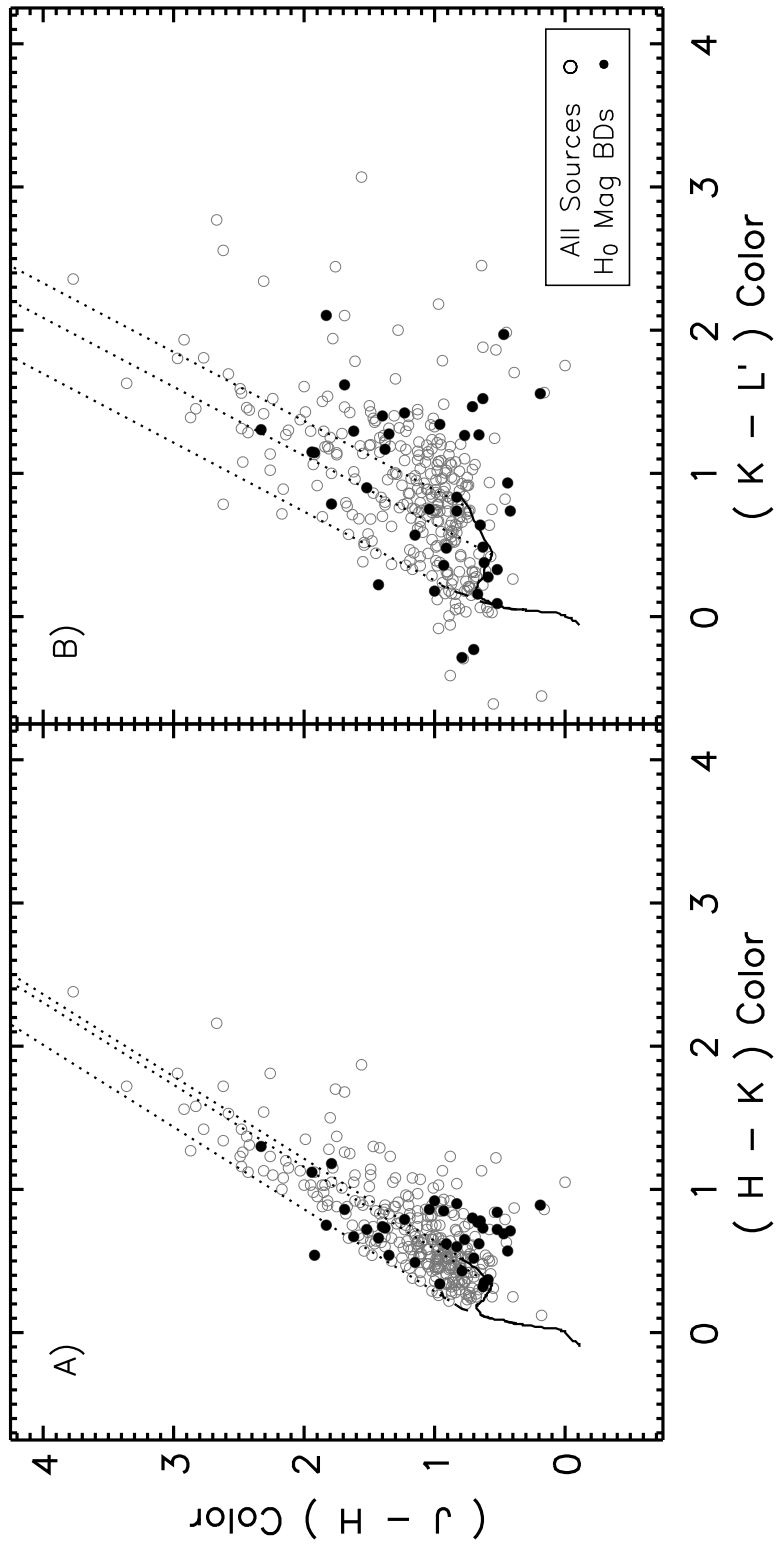
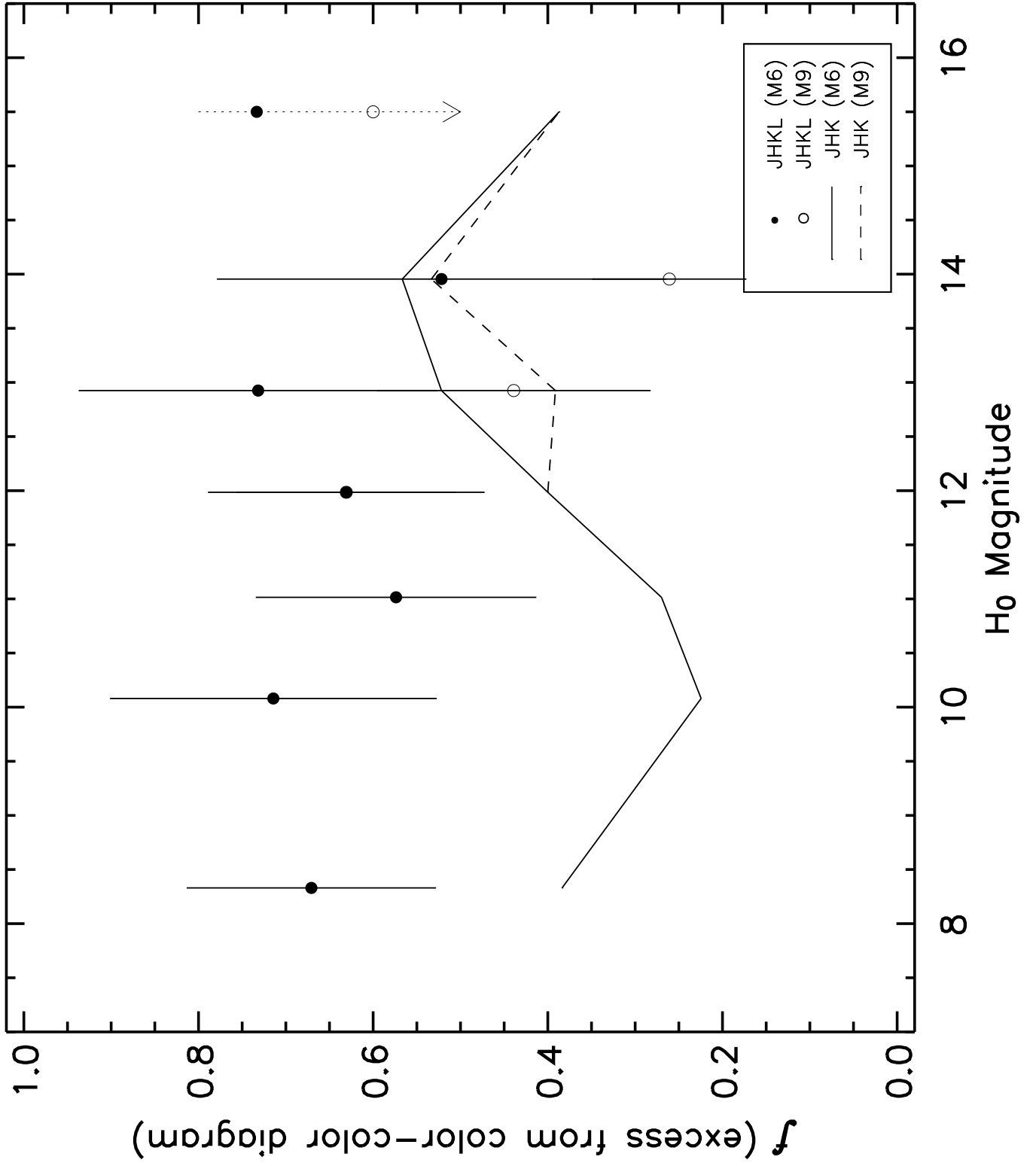
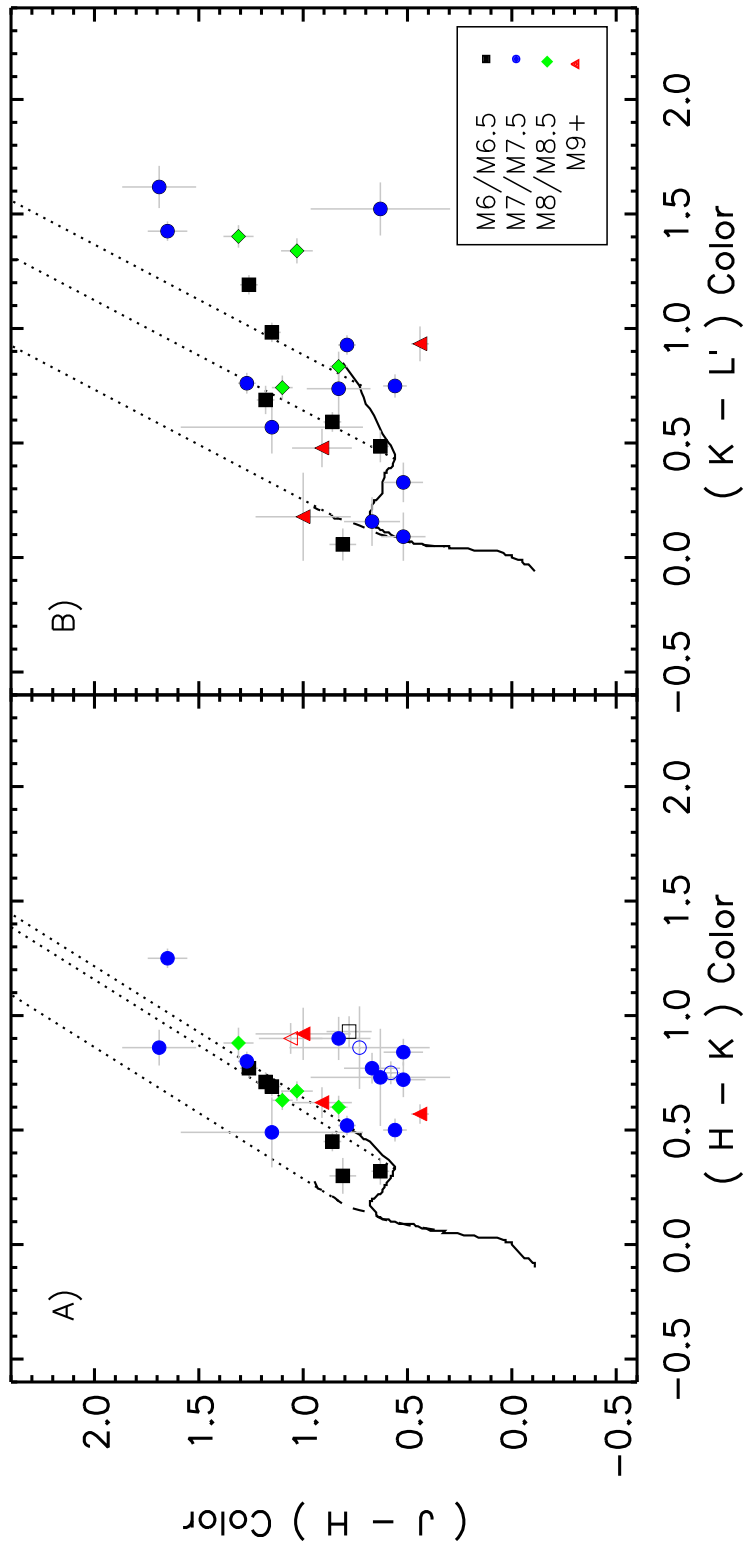


Figure 2 is included as jpeg file in the ASTRO-PH version.









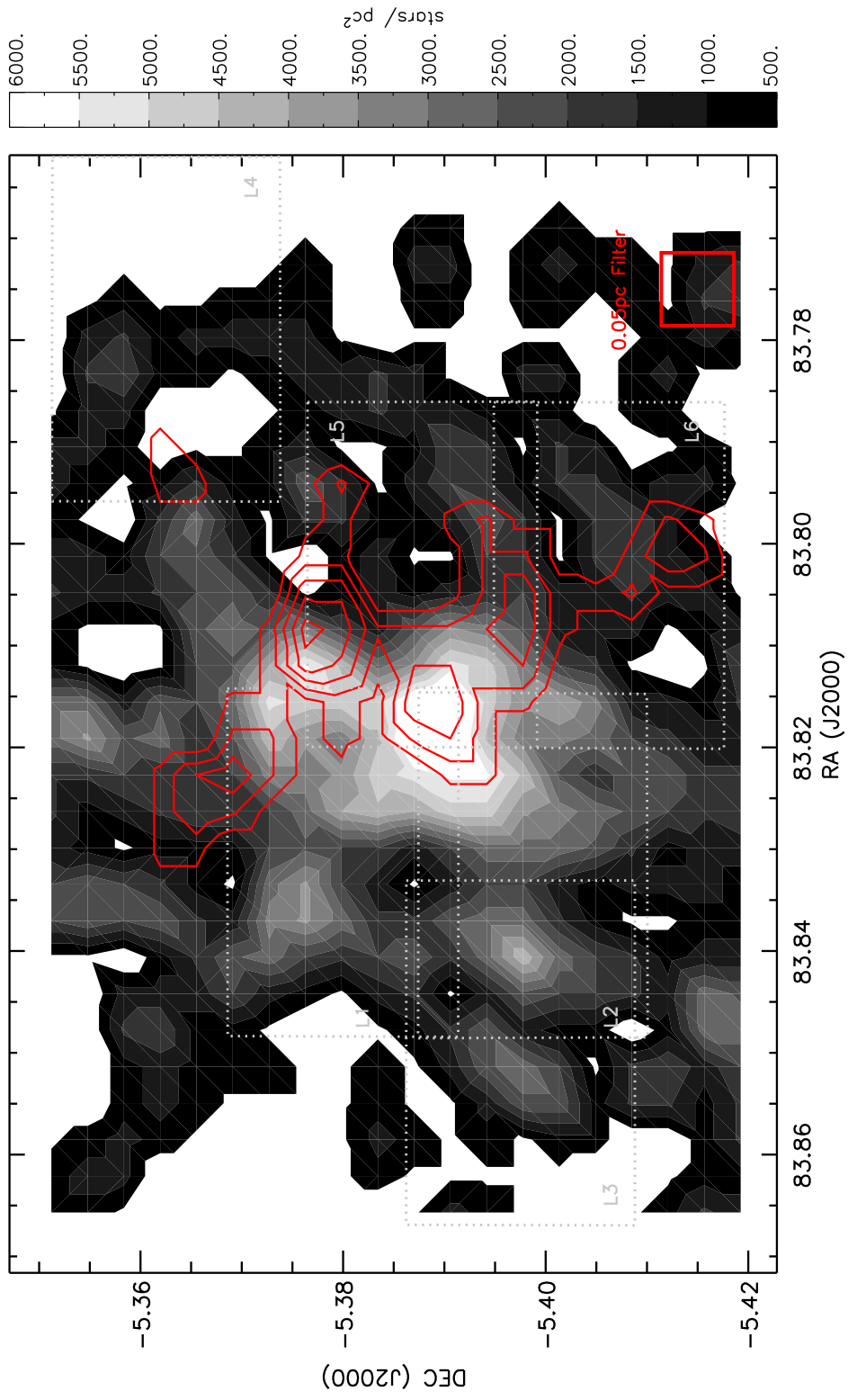


Table 1. Observational Details

Image Name	Date	Julian Date	RA (J2000)	DEC (J2000)	Nods Used	Total Exp. (min) ^(a)	FWHM (")
L1	2002-10-10	52557.242325	5:35:19.507	-5:22:47.95	60	29.70	0.53
L2	2002-10-10	52557.284110	5:35:19.580	-5:23:55.45	59	29.21	0.34
L3	2002-10-12	52559.242141	5:35:24.003	-5:23:51.06	59	29.21	0.85
L4	2002-10-12	52559.282716	5:35:06.943	-5:21:45.10	60	29.70	0.39
L5	2002-10-14	52561.357352	5:35:12.723	-5:23:16.17	59	29.21	0.48
L6	2002-12-19	52627.255228	5:35:12.749	-5:24:22.58	60	29.21	0.42

^(a)Total Exposure is derived from: Number of Nods * 2 (On+Off Chop) * 15 Chopping cycles * 9 coadds * 0.11 sec per frame.

Table 2. VLT 3.8 μ m Trapezium Catalog

No.	f_n (^a)	R.A. (J2000)	Dec. (J2000)	f_p (^b)	Image Information			Photometry			Cross References			
					Image	X Pixel	Y Pixel	Beam('')	L'	err	MLLA02	HC2000	H97	
1	9	05 35 04.174	-05 22 24.52	0	L4-033	274.916	1134.839	1.14	12.041	0.056				244
2	9	05 35 04.389	-05 21 23.51	0	L4-012	319.637	268.436	1.14	14.007	0.126				
3	1	05 35 04.956	-05 21 09.45	0	L4-032	439.672	68.905	1.14	10.767	0.019	00856			
4	1	05 35 05.583	-05 21 40.58	0	L4-011	572.784	510.949	1.14	14.428	0.132	00789			
5	1	05 35 06.175	-05 22 12.51	0	L4-001	698.199	963.988	1.14	10.811	0.019	00681	508	3064	
6	1	05 35 06.203	-05 21 36.06	0	L4-013	703.921	446.854	1.14	15.031	0.187	00796	601		
7	1	05 35 06.289	-05 22 02.75	0	L4-004	722.275	825.489	1.14	8.593	0.007	00716	538	286	
8	1	05 35 06.355	-05 22 11.63	0	L4-002	736.148	951.438	1.14	14.575	0.138	00685	509		
9	1	05 35 06.454	-05 22 07.61	0	L4-003	757.271	894.435	1.14	11.691	0.029	00700	526	287	
10	1	05 35 06.472	-05 21 18.97	0	L4-009	760.816	204.533	1.14	11.755	0.030	00837	636	288	
11	1	05 35 06.896	-05 22 09.31	0	L4-005	850.663	918.522	1.14	12.715	0.048	00692	521	298	
12	0	05 35 7.046	-05 22 17.06	0					99.000	-1.000	00667	497		
13	1	05 35 07.223	-05 21 34.64	0	L4-007	919.862	426.863	1.14	13.624	0.077	00803	603		
14	1	05 35 07.242	-05 22 03.97	0	L4-006	923.860	842.755	1.14	13.245	0.063	00711	534		
15	0	05 35 7.505	-05 21 45.93	0					99.000	-1.000	00772	718		

(^a)Detection/Photometry Flag. The value of this flag indicates if a known source was saturated (-13), fell into a negative chop image (-1) or was undetected (0); it also indicates the number of times a detected source was photometered (1..3), in which case the photometry is the mean of the set and the recorded error is the standard deviation. Additional values of this flag are (9) for previously undetected IR sources and (10) for previously unresolved IR source.

(^b)Astrometry Flag. For sources falling into image overlaps, the relative dispersion of the astrometry is recorded, otherwise the flag is set to 0. A flag of '1' indicates the relative dispersion was greater than 0.2''; a value of '2' indicates the repeated source's astrometry was better than 0.2''.

Note. — The complete version of this table is in the electronic edition of the Journal. The printed edition contains only a sample.

Note. — This table is available only on-line as a machine-readable table.

Table 3. Excess Fractions for Trapezium Sources from Color-Color Diagrams

Band	H_0		$M_{\odot}^{(a)}$		$N_{CMD}^{(b)}$ (b)	No L' (c)	Boundary (SpT)	JHK %	$JHKL'$ %	HKL' %
	Max	Min	Max	Min						
1	7.00	9.66	5.000	1.200	83	0	M6	38	67	66
2	9.66	10.50	1.200	0.570	49	0	M6	22	71	73
3	10.50	11.53	0.570	0.250	63	0	M6	27	57	60
4	11.53	12.44	0.250	0.130	70	0	M6	40	63	69
5	12.44	13.41	0.130	0.080	43	1	M6	52	73	76
6	13.41	14.50	0.080	0.045	34	7	M6	57	52	44
7	14.50	16.50	0.045	0.020	45	28	M6	39	73	71
5	M9	39	44	43
6	M9	53	26	30
7	M9	39	60	65
All L' Sources							M5	50	68	70
...							M6	39	67	68
...							M9	32	42	47

^(a)Conversion from H_0 Magnitude to solarmass using the 1 Myr isochrone from Baraffe et al. (1998)

^(b)Total VLT sources with HK photometry selected from Figure 3b that are not saturated or falling into negative chop images.

^(c)Number of CMD selected sources undetected at L' .

Table 4. Sub-Clusters in the Trapezium

Sub-Cluster	RA (J2000)	DEC (J2000)	Peak Density stars/pc ²	R ^(a) (pc)	N ^(b)	Comments
Trapezium Sub-Clusters ^(c)						
TSC-a	05:35:16.234	-05:23:25.19	7200.	0.08	93	Trapezium Core
TSC-b	05:35:15.734	-05:22:29.79	5600.	0.06	43	Near BNKL
TSC-c	05:35:21.689	-05:23:51.70	4400.	<0.05	16	
TSC-d	05:35:20.490	-05:22:33.72	3600.	0.05	20	
Deeply Embedded <i>K–L</i> Sub-Clusters ^(d)						
DESC-a	05:35:15.672	-05:23:24.92	2400.	0.05	14	Trapezium Core
DESC-b	05:35:14.090	-05:22:41.14	3200.	0.06	16	BNKL
DESC-c	05:35:17.739	-05:22:05.22	2400.	0.05	12	
DESC-d	05:35:13.989	-05:23:49.94	2400.	<0.05	10	Orion S.
DESC-e	05:35:12.264	-05:24:43.50	2000.	<0.05	8	

^(a)Sub-Cluster radius suggested by radial profile of candidates sources (low A_V or embedded).

^(b)Number of sub-cluster members within radius.

^(c)Trapezium sources defined by $J-H < 1.5$, which for a CTTS corresponds to approximately $A_V \sim 8$.

^(d)Embedded sources defined by $K-L < 1.5$ and L only sources.

This figure "lada.fig2.jpg" is available in "jpg" format from:

<http://arxiv.org/ps/astro-ph/0406326v1>